FULL PAPER

Dalton
www.rsc.org/dalton

One- and two-photon excited dual fluorescence properties of zinc(II) and cadmium(II) complexes containing 4-dipropylamino-benzaldehyde thiosemicarbazone

Zhao-Ming Xue,*[a] Yu-Peng Tian,*[a,b,c] Dong Wang[b] and Min-Hua Jiang[b]

[a] *Department of Chemistry, Anhui University, Hefei, 230039, China. E-mail: zmxue@ahu.edu.cn; yptian@ahu.edu.cn; Fax: 86-551-5106000*

[b] *State Key Laboratory of Crystal Materials, Shandong University, Jinan, 250100, China*

[c] *State Key Laboratory of Coordination Chemistry, Nanjing University, Nanjing, 210093, China*

Received 1st October 2002, Accepted 10th February 2003
First published as an Advance Article on the web 28th February 2003

A new ligand, 4-dipropylaminobenzaldehyde thiosemicarbazone (HL) and its complexes (ZnL_2, CdL_2), which exhibit intense two-photon excited (TPE) dual fluorescence using 800 nm laser pulses in the femtosecond regime, were synthesized and fully characterized. The measured power dependence of the fluorescence signals provides direct evidence for TPE. The two-photon excited dual fluorescence spectra were compared and contrasted with the corresponding results obtained from one-photon excitation. Emission peaks of the ligand and its complexes were assigned with the aid of PM3 calculations.

Introduction

Shortly after the experimental verification of two-photon absorption[1] by Kaiser and Garret with a CaF_2:Eu^{2+} crystal in 1961, two-photon processes have been used to create a number of chemical or physical processes including optical data storage,[2] optical waveguiding,[3] lithographic fabrication,[4] and fluorescence imaging.[5] In fluorescence imaging, two-photon excitation (TPE) has developed as an important alternative to traditional one-photon excitation (OPE) in fluorescence microscopy and spectroscopy.[6,7] The intrinsic advantages of two-photon excitation include reduced background fluorescence from fluorophores outside the focal volume, decreased photobleaching, inherent optical sectioning capability, and lower photodamage of sensitive biological samples.[8] Recently, selective recognition and *in situ* sensing of biologically important molecules using a dual fluorescent intramolecular charge transfer (ICT) fluorophore are of considerable significance in host–guest chemistry.[9–11]

This area, perceived until recently to be of only academic interest, is now offering numerous opportunities both for fundamental research and for new application development. However, most of the reported materials which exhibit a strong TPE fluorescence or OPE dual fluorescence are organic chromophores.[12–15] To our knowledge, metal complexes with strong two-photon absorption are less studied. The organic chromophore, 4-dipropylaminobenzaldehyde thiosemicarbazone, which is a π-electron delocalized system containing mixed sulfur and nitrogen donors, was considered and prepared in our laboratory for two-photon exciting dual fluorescence. Following the success of our initial work, we were particularly interested in further using it as a ligand to coordinate to transition metal ions to form metal complexes that show efficient TPE dual fluorescence. We selected Zn^{2+} and Cd^{2+} as the metal ions, which have d^{10} structures, to form metal complexes with the ligand. In this paper, we present the two-photon properties of the ligand and its complexes that exhibit intense two-photon excited dual fluorescence.

Theory

1 Two-photon excited fluorescence

TPE of a fluorophore involves the absorption of two photons in the same quantum event generating an electronically excited state, followed by the subsequent spontaneous emission of another (generally higher-energy) photon at the characteristic wavelength of fluorophore emission. This induced fluorescence signal displays a squared dependence on the exciting optical power. The basic equation relating the fluorescence signal FI_2 (in the absence of saturation, self-quenching, photobleaching, or stimulated emission) to the experimental parameters for TPE is given by eqn. (1):[16]

$$FI_2 = k(\Phi_2/2)n_2\sigma_2 l\rho_2^2 \quad (1)$$

where Φ_2 is the fluorescence quantum yield of the molecule, n_2 is the fluorophore number density, σ_2 is the two-photon absorption cross-section (cm^4 s), l is the path length, ρ_2 is the incident photon flux density in photons cm^{-2} s^{-1}), and k is a dimensionless constant that depends on the optical setup. The factor 2 in the denominator reflects the fact that two photons are required for each absorption event. Since TPE is essentially an instantaneous process, the peak incident photon flux density of a pulsed laser source ρ_{peak} determines the excitation rate.

2 Dual fluorescence

4-(*N*,*N*-Dimethylamino)benzonitrile (DMABN) is the prototype of a group of organic donor–acceptor compounds that can undergo intramolecular charge transfer (ICT) in the excited singlet state. In polar solvents, it exhibits dual fluorescence: apart from "normal" emission out of the locally-excited (LE) state, which is also present in the gas phase and in nonpolar solvents, in polar solvents a second, "anomalous", strongly red-shifted band is observed in the spectrum, attributed to a charge-transfer (CT) state. This phenomenon has been mostly explained by the twisted ICT (TICT) mechanism. In the "twisted intramolecular charge transfer" (TICT) model, a 90° twist of the dimethylamino group with respect to the phenyl ring was considered to have occurred in the CT state of DMABN. The dimethylamino group was thereby assumed to be electronically decoupled from the rest of the molecule: the "principle of minimum overlap". The CT/LE fluorescence quantum yield ratio Φ'(CT)/Φ(LE) increases with the efficiency of the ICT reaction.

Experimental

1 Chemicals

The new ligand (HL), and its complexes (ZnL_2 and CdL_2) were synthesized (Scheme 1) and fully characterized by elemental

DOI: 10.1039/b301589k

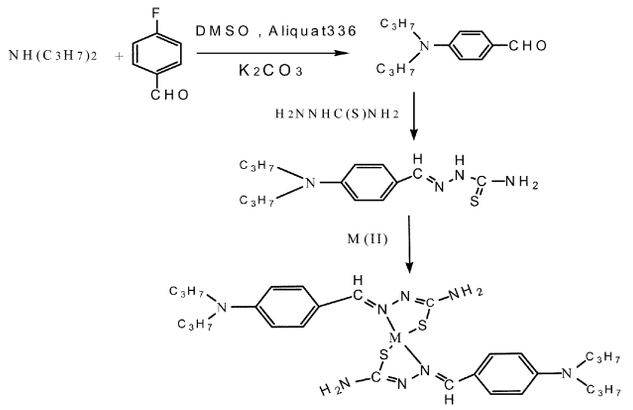

Scheme 1 Strategy of syntheses of HL and ML_2 (M = Zn or Cd).

analysis (Perkin-Elmer 240 elemental analyzer), MS (ZAB-HS mass spectrometer, FAB source), ^{1}H NMR (Bruker AM-500 spectrometer), IR (Nicolet FT-IR 170SX) and UV-Vis (UV-265 spectrophotometer). All the compounds are large π-electron delocalized systems containing mixed sulfur and nitrogen donors (Chart 1).

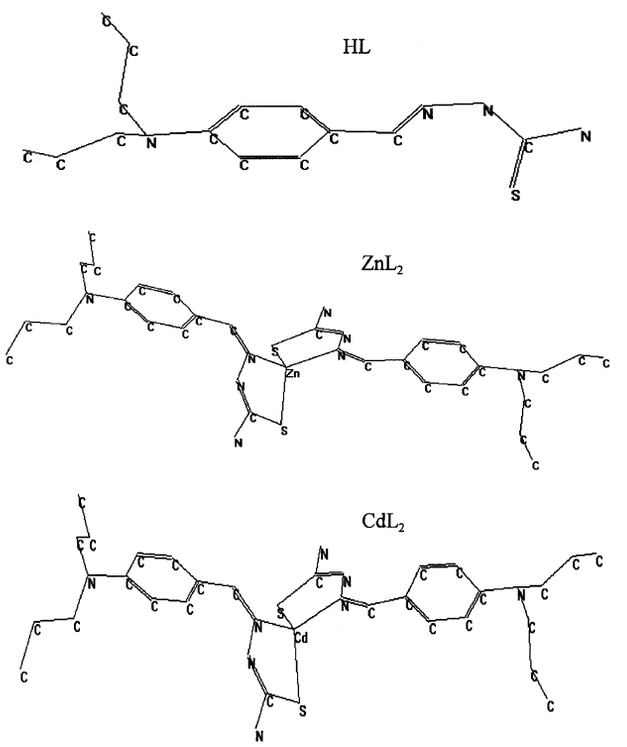

Chart 1

2 General procedures

The one-photon excited fluorescence measurements were carried out in DMF solutions and the spectra were collected with an Edingburg FLS920 spectrofluorimeter. No aggregation or self-absorption effects were observed up to 0.1 μmol L^{-1} solutions in the solvents studied. Therefore, we prepared 0.1 μmol L^{-1} sample solutions for absorption, emission, and quantum yield ratio Φ'(CT)/Φ(LE) studies.

The experimental configuration to investigate the two-photon induced fluorescence behavior, consisting of a femtosecond titanium–sapphire laser system, and an optical fiber-coupled CCD spectrophotometer is shown in Fig. 1. A regeneratively amplified titanium–sapphire mode-locked laser system (800 nm excitation, 76 MHz repetition rate, <200 fs pulse width, Coherent Mira900-D) was used to generate pulses.

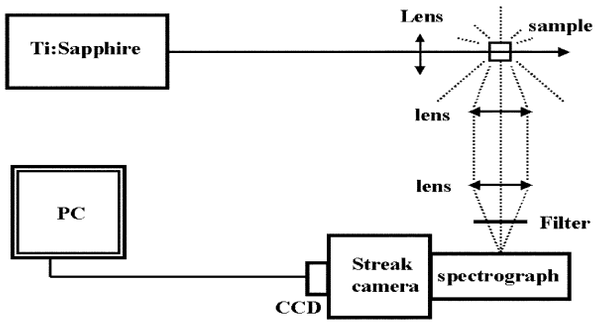

Fig. 1 Experimental set-up for investigation of the two-photon induced fluorescence behavior.

3 Synthesis of 4-dipropylaminobenzaldehyde

25 g (0.2 mol) of 4-fluorobenzaldehyde, 70.8 g (0.7 mol) of dipropylamine, 41.5 g (0.3 mol) of anhydrous potassium carbonate, and three drops of Aliquate-336 were introduced into a round-bottom flask fitted with a condenser. The mixture was stirred at 95 °C for 92 h, and after cooling to room temperature, it was poured into an ice–water mixture. The aqueous layer was extracted with dichloromethane and the organic layer washed twice with cold water. After solvent evaporation, the reddish oil was dissolved in 200 mL of diethyl ether and poured into 800 ml of 1 mol L^{-1} hydrochloric acid (HCl) in water. After stirring for 10 min, the aqueous layer was separated and neutralized using an aqueous sodium carbonate solution. Then 200 mL of dichloromethane was added, the organic layer separated, and dried with anhydrous sodium sulfate. The crude product was obtained as a brown oil after removing the solvent, yield 27 g (65%), and purified by decompression evaporation. The brown oil-like product was collected at 164–168 °C (3 mmHg).

4 Synthesis of 4-dipropylaminobenzaldehyde thiosemicarbazone (HL)

100 mmol of 4-Dipropylaminobenzaldehyde, 100 mmol of thiosemicarbazone, and 100 ml ethanol were introduced into a round-bottom flask fitted with a condenser. The mixture was refluxed for 4 h, cooled to room temperature, and then the product was precipitated. The crude product was filtered off and washed with ethanol three times. Then it was purified by crystallization from ethanol. A yellow powder product was obtained and dried *in vacuo* over P_2O_5. The total yield of the product was 60%, mp 201–202 °C. Anal. Calc. for $C_{14}H_{22}N_4S$: C, 60.43; H, 7.91; N, 20.14. Found: C, 60.80; H, 8.21; N, 19.87%. MS: m/z = 279 (M^+). Crystals of HL were isolated by slow evaporation of an ethanol solution.

5 Syntheses of ML_2 (M = Zn or Cd)

$M(OAc)_2 \cdot nH_2O$ (M = Zn(II), Cd(II)) (1 mmol) and HL (2 mmol) was dissolved in ethanol (50 ml). After refluxing for 4 h, the mixture was cooled to room temperature. The precipitate was thoroughly washed with ethanol three times and dried *in vacuo* over P_2O_5 (yield 90%).

Anal. Calc. for $C_{28}H_{42}N_8S_2Zn$: C, 54.22; H, 6.83; N, 18.07%. Found: C, 54.20; H, 6.81; N, 18.12%. Calcd. for $C_{28}H_{42}N_8S_2Cd$: C, 50.40; H, 6.34; N, 16.79%. Found: C, 50.34; H, 6.38; N, 16.82%.

Results and discussion

1 Absorption

The electronic absorption spectra of HL, ZnL_2 and CdL_2 (c_0 ~10^{-5} mol L^{-1}), shown in Fig. 2, were measured in DMF solutions.

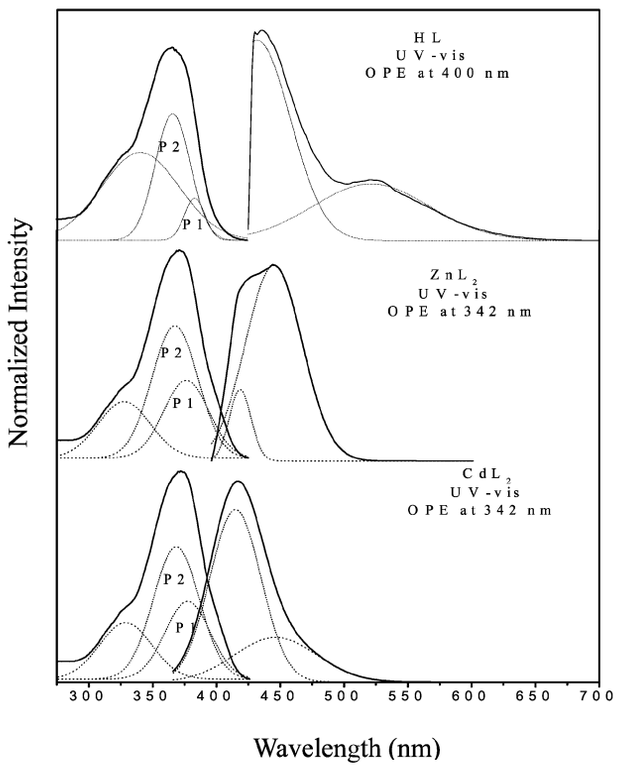

Fig. 2 Room-temperature absorption (left) and emission spectra (right, excited by one-photon) of HL, ZnL_2 and CdL_2 in DMF solution. The dotted lines represent the approximate Gaussian components of the spectra.

All the compounds (HL, ZnL_2 and CdL_2) exhibit essentially the same absorption profile: an intense and low-lying (near UV region) absorption band. The large molar absorption coefficients ($\log\varepsilon$ 4–5) are indicative of highly π-conjugated systems. If the sum of Gaussian-shaped bands corresponding to the different types of transition is reproduced with good accuracy, three bands in the range 275–425 nm, with tailing at long wavelengths can be observed. There is no linear absorption in the wavelength range ~500–800 nm. For HL, there is a weak band (P1) around 384 nm and a stronger band (P2) around 365 nm. The energy gap ΔE(P1, P2) between P1 and P2 is smaller for CdL_2 (378, 369 nm) and, in the case of ZnL_2 (376, 370 nm), the two bands strongly overlap, the vibrational structure of P1 being still visible on the long-wavelength slope of the absorption spectrum at *ca.* 380 nm (Fig. 2). The result shows that the energy gap ΔE(P1, P2) becomes smaller upon coordination of the ligand to metal ions. This is because after HL is coordinated to metal ions it forms a five-membered ring and a wider π-conjugated system, the electron affinity of the benzaldehyde moiety is reduced, and the energy gap ΔE(P1,P2) is decreased. The effectiveness of Zn^{2+}on the ligand is stronger than that of Cd^{2+}.

2 One-photon excited dual fluorescence

The one-photon steady-state emission spectra of HL, ZnL_2 and CdL_2 (c_0 =1.0 × 10^{-7} mol L^{-1}), shown in Fig. 2, were measured in DMF solutions.

HL, ZnL_2 and CdL_2 emit a blue color with dual peaks and a large Stokes shift (~50–70 nm) when irradiated (one-photon processes) by UV at 400, 342 and 342 nm, respectively, in DMF solutions. There is an overlap in the wavelength range 350–450 nm between absorption and emission spectra. The characteristic benzaldehyde moiety bands have peaks at 523 and 430 nm for HL, 445 and 418 nm for ZnL_2, and 447 and 416 nm for CdL_2. They show the quantum yield ratio Φ'(CT)/Φ(LE) order (c_0 = 1.0 × 10^{-7} mol L^{-1}) as ZnL_2 (7.01) > HL (0.79) > CdL_2 (0.41).

3 Spectra of two-photon excited dual fluorescence

3.1 Steady-state spectra. HL, CdL_2 and ZnL_2 excited at 800 nm in DMF solutions (1.0 × 10^{-2} mol L^{-1}) yielded the dual fluorescence (TICT, LE) spectra displayed in Fig. 3. The characteristic benzaldehyde moiety bands had peaks at 475 and 430 nm for HL, 535 and 464 nm for ZnL_2, and 500 and 450 nm for CdL_2. The LE peak of HL is at the same position as that observed with OPE at 400 nm, and the LE peaks of ZnL_2 and CdL_2 are shifted towards longer wavelengths. They show the quantum yield ratio (Φ'(CT)/Φ(LE)) order: HL (1.41) > CdL_2 (0.40) > ZnL_2 (0.27). Most of the LE emission wavelengths are separated from the linear absorption band, *i.e.*, there is a large Stokes shift (~50–90 nm).

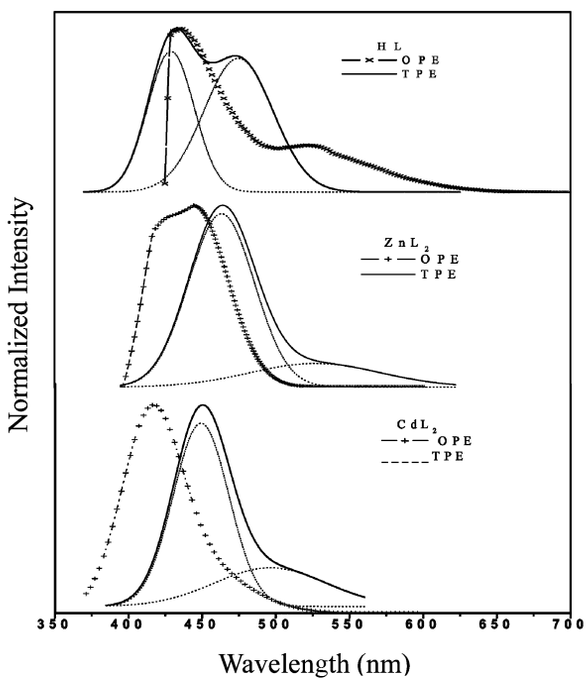

Fig. 3 Room-temperature normalized steady-state OPE (c_0 = 1.0 × 10^{-7} mol L^{-1}) and TPE (c_0 = 1.0 × 10^{-2} mol L^{-1}) fluorescence emission spectra of HL, ZnL_2 and CdL_2 in DMF solution.

3.2 Excitation power dependence. The power dependence of the fluorescence detected at the LE maximam wavelength for each species was determined from a log–log plot of the fluorescence signal *vs.* incident peak photon flux density shown in Fig. 4. For photon flux densities < ~14.70 × 10^{28} for HL, ~15.63 × 10^{28} for ZnL_2 and ~16.73 × 10^{28} photons cm^{-2} s^{-1} for

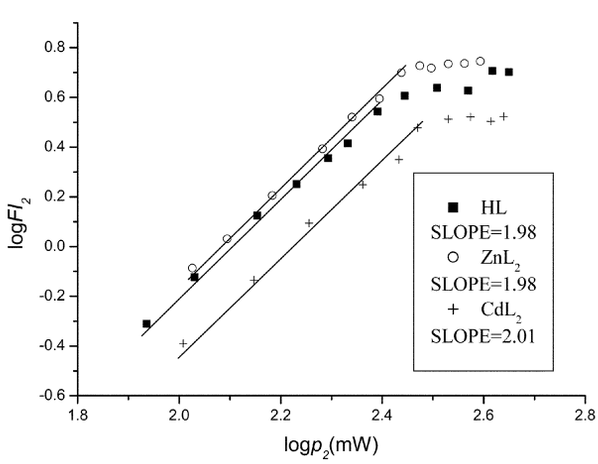

Fig. 4 Log–log plot of the fluorescence emission of HL, ZnL_2 and CdL_2 *vs.* the incident photon flux density for TPE excitation at 800 nm (1 mW = 5.619 × 10^{26} photons cm^{-2} s^{-1}).

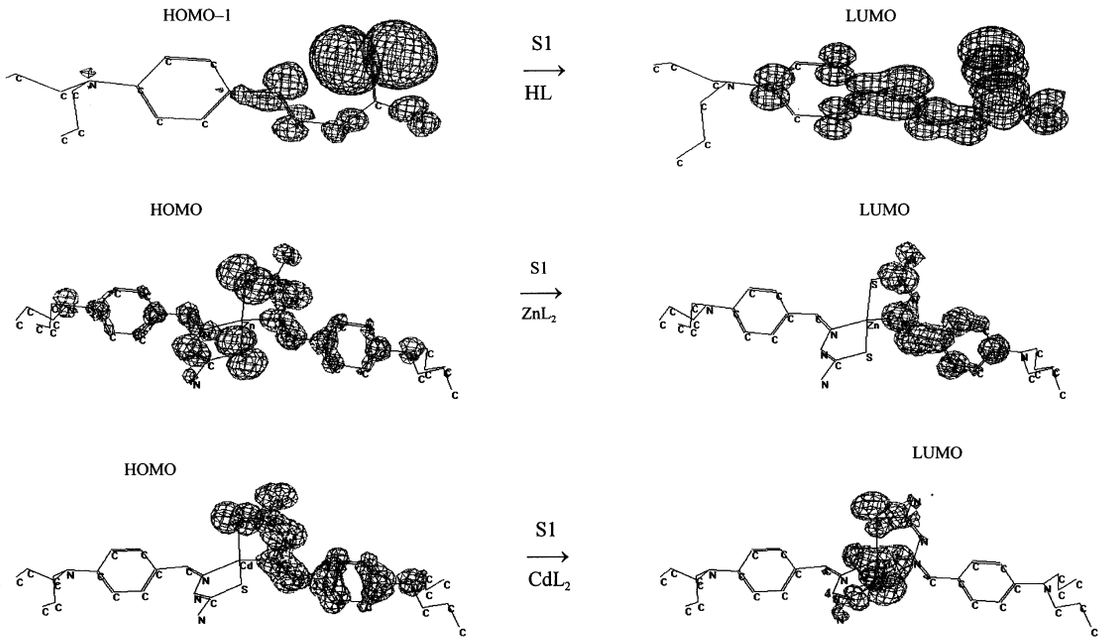

Fig. 5 The occupied and unoccupied molecular orbitals of the lowest energy singlet state S1.

CdL_2, respectively, the induced fluorescence obeyed a power-squared intensity dependence as indicated by the measured slope (shown in Fig. 4), thereby confirming the existence of TPE. However, a decrease in the apparent power exponent was observed for larger irradiances. All measurements were carried out at lower intensity levels at which deviations from the second-order power law were absent.

Comparing the LE peak of the TPE induced fluorescence spectrum with that of the OPE induced fluorescence spectrum, one can see that there is a 45 nm red shift for ZnL_2 and 34 nm red shift for CdL_2, which can be explained by a reabsorption effect. As mentioned above, there is an overlap between the linear absorption spectrum and one-photon excited fluorescence spectrum for each compound. Since the one-photon excited fluorescence spectrum was measured at a very low concentration ($c_0 = \sim 1.0 \times 10^{-7}$ mol L^{-1}), the reabsorption effect can be neglected in this instance. However, since the two-photon excited fluorescence spectrum was measured at a much higher concentration ($c_0 = \sim 1.0 \times 10^{-2}$ mol L^{-1}), the reabsorption effect greatly decreased the blue side of the TPE fluorescence spectrum.

The blue LE emission spectra of HL observed upon 800 nm excitation were in general agreement with the fluorescence spectra excited by OPE at 400 nm. This fact, coupled to energy conservation considerations, indicates a simultaneous absorption of two 800 nm photons. Direct evidence for the TPE phenomenon was provided by the measured power-squared dependence of the induced fluorescence intensity on the incident 800 nm photon flux density.

On the basis of the fact that the LE emission spectra of HL are nearly the same for OPE and TPE, one may conclude that in both cases the fluorescence LE emission of each compound is predominantly from the same S_1 singlet state. As there is a considerable Stokes shift between the pump wavelength λ_0 for OPE (or $\lambda_0/2$ for TPE) and the emission wavelengths, the excited molecules must relax to the lowest excited state of the S_1 singlet band before they start to emit the fluorescence. For this reason, there must be a definite time delay between the moment at which the absorption takes place and emission starts. On the other hand, the upper state of the molecule transition for one-photon absorption and for two-photon absorption may be different. For example, in centrosymmetric structures, they are different because the OPE allows only $g \longrightarrow u$ transitions, whereas the TPE produces a $g \longrightarrow g$ transition. For this reason, the two-photon excitation/absorption spectra might be drastically different from the corresponding linear excitation/absorption spectra (in the absorbing photons energy scale) for a given solution sample. Based on these considerations, one can explain the differences between TPE and OPE fluorescence quantum yield ratio orders and features.

The TPE fluorescence is clearly saturated at higher flux densities, thereby establishing an upper limit for quantitative TPE microscopy of $\sim 14.7 \times 10^{28}$, $\sim 15.63 \times 10^{28}$ and $\sim 16.73 \times 10^{28}$ photons cm^{-2} s^{-1} for HL, ZnL_2 and CdL_2, respectively. The apparent saturation may be attributed to a variety of nonlinear optical processes, such as stimulated emission,[17] excited-state absorption,[18] photolysis,[19] and ground-state depletion.[20] Non-perturbative nonlinear phenomena caused by a high instantaneous field strength become important only at intensities $>10^{31}$ photons cm^{-2} s^{-1}. Stimulated emission could also be excluded, since there was no overlap of the excitation wavelength of 800 nm with the fluorescence. Fluorescence saturates at the limit of one transition per pulse per fluorophore. For a two-photon process, saturation occurs when $\sigma_2 \rho^2_{peak} \tau_{pulse} \approx 1$. Assuming a typical value of $\sigma_2 = 1.0 \times 10^{-47}$ cm^4 s photon^{-1} for HL or ML_2, $\tau_{pulse} \approx 200$ fs, and a threshold value for the saturation peak intensity of $\rho_{peak} \approx 1.0 \times 10^{29}$ photons cm^{-2} s^{-1} (Fig. 4), the above relation yields ~0.03. Since OPE at 800 nm can be neglected, this result indicates that ~3% of molecules in the focal spot are excited per laser pulse in TPE. Therefore, ground-state depletion cannot have been the dominant contribution to the observed saturation. In conclusion, quenching of the excited singlet state by excited-state absorption at high power levels is the most likely cause for the observed deviation from the simple power law.

4 PM3 Calculations

The electronic structures and spectra of HL, CdL_2 and ZnL_2 were investigated by semiempirical PM3/SCI calculation.[21] The molecular structures were those obtained from PM3 calculations. The nodal patterns for the occupied and unoccupied molecular orbitals of the lowest energy singlet state S1 are shown in Fig. 5. The calculated absorption maxima, oscillator strengths, and character of the lowest energy singlet states of HL, CdL_2 and ZnL_2 are summarized in Table 1. Among the

Table 1 Calculated (PM3/SCI) absorption maxima, oscillator strengths and character of S1 [a]

HL				ZnL_2			CdL_2		
	λ_{max}/nm	f	Character	λ_{max}/nm	f	Character	λ_{max}/nm	f	Character
S1	536	0.0006	HOMO−1 →LUMO	380	0.5577	HOMO →LUMO	387	0.0056	HOMO →LUMO
	[535]	[0.0006]	[HOMO−1 →LUMO]	[387]	[0.7524]	[HOMO−1 →LUMO]	[391]	[0.4532]	[HOMO−1 →LUMO]
S1 energy/eV		−2830.9373 [−2830.4355]			−5663.1070 [−5662.8152]			−5656.0695 [−5654.1285]	
Barrier (0 → 90°)/kJ mol^{-1}	48.4			28.1			187.1		

[a] Values for *trans* (0°) and *cis* (90°) (in square brackets) forms.

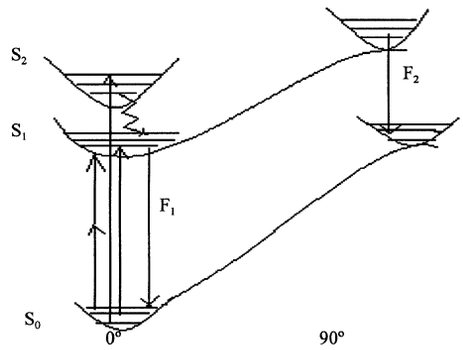

Fig. 6 Energy-level diagram for HL.

three compounds, the lowest energy singlet state is largely π,π* in character and possesses the lowest oscillator strength for HL.

Since rotation about the amide C–N bond has been implicated in the formation of the singlet state responsible for TICT (F2) fluorescence (shown in Fig. 6), we have investigated the effect of this bond rotation on the energies of the lowest singlet states of HL, CdL_2 and ZnL_2. Vertical transitions were calculated at 90° rotation about this bond, using the PM3 minimized geometries. The calculated ground-state energies were added to the vertical transitions. As shown in Table 1, the calculated barrier for rotation of S1 is 48.4 kJ mol^{-1} for HL, 28.1 kJ mol^{-1} for ZnL_2 and 187.1 kJ mol^{-1} for CdL_2. The calculated barrier order is reversed relative to the quantum yield ratio order since CdL_2 > HL > ZnL_2. Based on the different barriers, one can thus rationalize the OPE fluorescence quantum yield ratio order.

A singlet-state diagram that can account for the fluorescence behavior of HL is shown in Fig. 6. The LE (F1) fluorescence observed upon excitation in the long-wavelength tail of the absorption band (Fig. 2) is attributed to a lowest singlet (S1) π,π* state. S1 is also a precursor of F2 fluorescence. The large Stokes shift for F2 fluorescence is indicative of a large change in geometry prior to fluorescence. A 90° twisting about the amide C–N bond in HL, ZnL_2 and CdL_2 is required for the formation of the TICT state responsible for F2 fluorescence. There is a considerable barrier for dipropylamino twisting from 0 to 90°. The lower the barrier, the higher the quantum yield ratio.

Acknowledgements

This work was support by a grant for the State Key Program of China (G1998061402), the National Natural Science Foundation of China (29871001, 20071001,50272001), and the Education Department of Anhui Province.

References

1 W. Kaiser and C. G. B. Garret, *Phys. Rev. Lett.*, 1961, **7**, 229.
2 S. Kawata and Y. Kawata, *Chem. Rev.*, 2000, **100**, 1777.
3 S. J. Frisken, *Opt. Lett.*, 1993, **18**, 1035.
4 W. H. Zhou, S. M. Kuebler, K. L. Braun, T. Y. Yu, J. K. Cammack, C. K. Ober, J. W. Perry and S. R. Marder, *Science*, 2002, **296**, 1106.
5 K. D. Belfield, K. J. Schafer, Y. Liu, X. B. Ren and E. W. V. Stryland, *J. Phys. Org. Chem.*, 2000, **13**, 837.
6 K. Svoboda, W. Denk, D. Kleinfeld and D. W. Tank, *Nature*, 1997, **385**, 161.
7 J. Bewersdorf, R. Pick and S. W. Hell, *Opt. Lett.*, 1998, **23**, 655.
8 W. Denk, D. W. Piston and W. W. Webb, in *Handbook of Biological Confocal Microscopy*, New York, Plenum Press, 1995, p. 445.
9 B. Dietrich, D. L. Fyles and J. M. Lehn, *Helv. Chim. Acta.*, 1979, **62**, 280.
10 F. P. Schmidtchen and M. Berger, *Chem. Rev.*, 1997, **97**, 1609.
11 P. A. Gale, *Coord. Chem. Rev.*, 2001, **213**, 79.
12 Y. Ren, Q. Fang, W. T. Yu, H. Lei, Y. P. Tian, M. H. Jiang, Q. C. Yang and T. C. W. Mak, *J. Mater. Chem.*, 2000, **10**, 2025.
13 G. Y. Zhou, X. M. Wang, D. Wang, C. Wang, X. Zhao, Z. S. Shao and M. H. Jiang, *Opt. Laser Technol.*, 2001, **33**, 209.

14 Y. V. Il'ichev, W. Kulhnle and K. A. Zachariasse, *J. Phys. Chem. A*, 1998, **102**, 5670.
15 F. Y. Wu, L. H. Ma and Y. B. Jiang, *Anal. Sci.*, 2001, **17**, 1801.
16 C. Xu and W. W. Webb, *J. Opt. Soc. Am. B.*, 1996, **13**, 481.
17 J. Kusba, V. Bogdanov, I. Gryczynski and J. R. Lakowicz, *Biophys. J.*, 1994, **67**, 2024.
18 D. J. Bradley, M. H. R. Hutchinson, H. Koetser, T. Morrow, G. H. C. New and M. S. Petty, *Proc. R. Soc. London A*, 1972, **328**, 97.
19 L. Brand, C. Eggeling, C. Zander, K. H. Drexhage and C. A. M. Seidel, *J. Phys. Chem. A*, 1997, **101**, 4313.
20 C. Xu, W. Zipfel, J. B. Shear, R. M. Williams and W. W. Webb, *Proc. Natl. Acad. Sci. USA.*, 1996, **93**, 10763.
21 F. D. Lewis and T. M. Long, *J. Phys. Chem. A*, 1998, **102**, 5327.